

Accepted by 30th International Symposium on Combustion

LEAN OR ULTRA LEAN STRETCHED PLANAR METHANE/AIR FLAMES

Zhongxian Cheng¹, Joseph A. Wehrmeyer, and Robert W. Pitz
Mechanical Engineering Department, Vanderbilt University
Box 1592 Station B, Nashville, TN 37235, USA
(Fax: 1-615-343-6687, E-mail: zhongxian.cheng@vanderbilt.edu)

PID 29840

Lean Stretched Planar Methane/Air Flames

¹ Corresponding Author

Abstract

Lean premixed combustion has potential advantages of reducing pollutants and improving fuel economy. In some lean engine concepts, the fuel is directly injected into the combustion chamber resulting in a distribution of lean fuel/air mixtures. In this case, very lean mixtures can burn when supported by hot products from more strongly burning flames. This study examines the downstream interaction of opposed jets of a lean-limit CH₄/air mixture vs. a lean H₂/air flame. The CH₄ mixtures are near or below the lean flammability limit. The flame composition is measured by laser-induced Raman scattering and is compared to numerical simulations with detailed chemistry and molecular transport including the Soret effect. Several sub-limit lean CH₄/air flames supported by the products from the lean H₂/air flame are studied and a small amount of CO₂ product (around 1% mole fraction) is formed in a “negative flame speed” flame where the weak CH₄/air mixture diffuses across the stagnation plane into the hot products from the H₂/air flame. Raman scattering measurements of temperature and species concentration are compared to detailed simulations using GRI-3.0, C₁ and C₂ chemical kinetic mechanisms, with good agreement obtained in the lean limit or sublimit flames. Stronger self-propagating CH₄/air mixtures result in a much higher concentration of product (around 6% CO₂ mole fraction) and the simulation results are sensitive to the specific chemical mechanism. These model-data comparisons for stronger CH₄/air flames improve when using either the C₂ or the Williams mechanisms.

Keywords: hot products; ultra lean; sub-limit; counterflow flames; Raman scattering

1. Introduction

Lean combustion is currently under investigation due to its potential advantages in limiting thermal NO_x emissions and in reducing fuel consumption. It has been used in gas turbines and direct injection spark ignition (DISI) engines. But a critical problem is that lean combustion tends to produce unburned hydrocarbon pollutants. For example, in DISI engines, ultra-lean combustion is achieved by charge stratification. The fuel/air mixture is inhomogeneous, leading to the simultaneous formation of lean, rich and stoichiometric regions. For the inhomogeneous reactants, Haworth et al. [1] simulated turbulent inhomogeneous combustion in DISI engines and found that hydrocarbon-rich fragments and oxidizer penetrate behind the primary heat-release zone to form a secondary reaction zone. Flames occurring in an inhomogeneously mixed fuel and air region are examples of partially premixed combustion. Some of this partially premixed mixture is so lean that it doesn't burn. But this ultra lean mixture may still react if hot products interact with it. That is, under certain conditions, the lean mixture region can burn and thus reduce the potential pollutants. The interaction of lean mixture with hot products needed to maintain the lean region burning is the focus of this work.

Partially premixed flames have been studied widely. In particular, the downstream interaction between two premixed streams was investigated by Sohrab et al. [2]. Most practical flames are stretched. The stretch effect combined with other aspects such as the effect of Lewis number or curvature will modify flame structure significantly [3, 4]. Considering the various conditions that exist simultaneously in inhomogeneous fuel/air reaction, a set of CH₄/air flames with a wide range of equivalence ratios and stretch rates impinging upon downstream hot products are studied experimentally and numerically. The opposed jet burner generates counterflow flames that are widely used to study chemical kinetics and species transport under

aerodynamic stretch. Using the opposed jet flames, partially premixed CH₄/air versus air flame structures were investigated [5, 6]. Lean partially premixed CH₄ and C₃H₈ flame structures versus hot products have also been investigated [7, 8]. In general, premixed flames [9, 10] are much less sensitive to stretch than diffusion flames [11]. In the present work, stretch effects on the flame structure of the downstream interaction between hot products and lean CH₄/air mixtures are studied with Raman scattering and detailed transport, complex chemistry numerical simulations.

2. Experimental System and Flames Examined

Measurement of major species and temperature are made along the centerline of an opposed jet burner using a nonintrusive Raman diagnostic system. The Raman system is the same as used previously and the details are given in [4, 8]. Number density measurements of major species are directly related to their spontaneous Raman signal strengths, and since all major species are measured the total number density of the local gas mixture is obtained and related to temperature via the ideal gas law (assuming pressure is 1 atm). For the present work the opposed jet burner has been modified by inserting honeycomb metal “flow straighteners” into both nozzles. These inserts have 0.8 mm honeycomb cells that are 19 mm in length. The inserts provide a very uniform exit velocity profile for both nozzles, as verified by hot wire anemometry traverses in nonreacting flow. In addition the new honeycomb metal inserts do not cause flame attachment of either H₂/air or hydrocarbon-air flames. The opposed jet burner was designed by Seshadri et al. [12] and has been used extensively for hydrogen- and hydrocarbon-fueled diffusion flames and for hydrocarbon-fueled premixed flames. With the honeycomb inserts, rather than wire screens, it can be used also for lean H₂/air premixed flames.

Eight flames, which are classified into three groups, are investigated by experiment and numerical simulation. All three groups have 300K inlet conditions for both jets. Group A includes three flames of CH₄/air mixtures, all with an equivalence ratio 0.68, versus lean H₂/air mixtures at stretch rates of 90, 140 and 210 s⁻¹. Group B includes three flames of CH₄/air mixtures, all with ϕ of 0.54, versus lean H₂/air mixtures at stretch rates 90, 140 and 210 s⁻¹. Group C includes two ultra lean sub-limit flames of CH₄/air mixtures ($\phi=0.33$ or 0.43) versus lean H₂/air mixtures at a stretch rate 140 s⁻¹. The maximum Reynolds number of jet flow is 1600 at stretch rate 210 s⁻¹. All of the lean H₂/air mixtures have the same ϕ of 0.28 and the calculated OH, O and H mole fractions for the H₂/air flames are of the order of 10⁻³, 8x10⁻⁴ and 5x10⁻⁴, respectively. This equivalence ratio is chosen to cause the lean H₂/air flame to be detached from the exit of the burner but still be separated from the upstream CH₄/air flame. CH₄ is a good alternate fuel because of its well-known chemical kinetics. Similar work has already been performed for planar C₃H₈/air flames versus hot products, but problems were encountered with the opposed jet burner used at the time [7]. Because premixed H₂/air has a fast burning velocity and tends to attach to the mesh screen or sintered metal plate at the nozzle exit (used to provide a top hat velocity profile), the boundary conditions were not well established [7]. Here a lean H₂/air flame with well established boundary conditions is used to generate hot products so that only high temperature water vapor, O₂ and N₂ impinge upon the hydrocarbon flame. Thus any CO₂ formed must come from the downstream interaction of the methane fuel and the hot products. The CO₂ is an indicator of the amount of CH₄ fuel that is burned.

3. Numerical Simulations and Mechanisms

Numerical flame simulation is performed with “OPPDIF” [13]. Detailed chemical kinetic mechanisms and transport data are used for numerical predictions. Four different chemical kinetic mechanisms are used for methane flames: one which models hydrocarbons with only one carbon atom (C_1) [14], one which models hydrocarbons containing up to two carbon atoms (C_2) [14], GRI-3.0 [15], and Williams et al. [16].

4. Results and Discussion

Experimental results from the Raman scattering measurement are achieved based on relevant calibration curves obtained across a wide equivalence ratio range from H_2 -air, H_2 -CO-air and H_2 -CO₂-air flames above a 25 mm diameter Hencken calibration burner, where chemical equilibrium is assumed at some distance downstream of the burner surface. Each opposed jet flame is modeled with the four detailed chemical kinetic mechanisms. Comparisons between experimental results and numerical simulation are performed for each flame.

Figure 1 shows a set of Raman spectral graphs from the flame: CH_4 -air ($\phi=0.68$) versus H_2 -air ($\phi=0.28$). They are two representative spectra from different locations along the centerline of the opposed jet burner. Each spectrum is the result of a 600 laser pulse accumulation of light signals onto the CCD, and each spectrum has background luminosity subtracted. It is found that all laser-induced background levels are very low for the lean premixed flames examined. The spatial resolution of the Raman measurement is 0.2 mm [8]. CO signals are detected in the flames but with too much uncertainty to be quantified.

At a given temperature and pressure, the flammability limit defines the equivalence ratio regime beyond which no flame will propagate. The lean flammability limits of CH_4 /air and

H₂/air mixture are 5% (fuel mole fraction) or ϕ of 0.5 and 4% or ϕ of 0.10, respectively [17]. By definition, the flammability limit is independent of external parameters [3]. The determination of flammability limit should be based on a stretchless adiabatic flame. Usually the limit is determined from the stretched flame data extrapolated to zero stretch rate [3], although this approach is disputed by Ju et al. [18]. All flames studied in this work are stretched premixed flames and their extinction limits depend on the mixture equivalence ratio, stretch rate, preferential diffusion (Lewis number effect) and heat loss.

4.1. Group A: stretched CH₄/air mixture with $\phi=0.68$ vs. hot products

For $\phi=0.68$, the CH₄/air mixture is above the lean flammability limit and forms a self-propagating flame at low stretch rate because of its sufficient strength. The aerodynamic stretch rate varies from 90 s⁻¹ to near an extinction limit, 210 s⁻¹. When the stretch rate is below some stretch rate (e.g. 140 s⁻¹), the flames are relatively strong. Such a flame structure is shown in Fig. 2. Near the extinction condition ($\kappa=210$ s⁻¹), the flames become very weak and almost invisible, even though the equivalence ratio is still 0.68. The flame structure is given in Fig. 4.

Experimental measurements and numerical predictions of temperature and reactant concentrations are compared in Fig. 2 for the methane-air ($\phi=0.68$) mixture vs. hot products at stretch rate $\kappa=140$ s⁻¹. The dashed line indicates the stagnation plane from modeling where the axial velocity is zero. As seen from the experimental data, a premixed “positive flame speed” flame exists on the CH₄/air side of the stagnation plane [2]. The uncertainties caused by shot noise are negligible and overall uncertainty for various species and temperature is about 3%. The representative error bars are shown in the Fig. 2. The results shown in Fig. 2 are from the Williams mechanism. The flame location is determined by fresh reactants velocity and local

laminar flame speed. For a particular equivalence ratio (i.e., $\phi=0.68$), the laminar flame speed almost doesn't change vs. stretch, so for higher reactant velocity indicated by higher stretch rate, the closer the flame location is to the stagnation plane. It is found that experimental profiles of all the major species and temperature match very well to the numerically predicted profiles by the Williams and C₂ mechanisms. The CH₄/air flame is located about 3.5 mm away from the top jet and the lean H₂/air flame is located downstream 8 mm from the top jet. The stagnation plane is located near the middle of the two jet exits. The peak flame temperature is close to 1800 K. About 6% CO₂ mole fraction is formed in the post flame zone. Further it is found that the peak temperature and the peak CO₂ concentration are not strongly influenced by the change in stretch rate κ .

Numerical predictions are performed with the four different chemical mechanisms and are shown in Fig. 3. From Fig. 3 on the CH₄/air flame side, the Williams and C₂ mechanisms demonstrate a relatively fast flame speed; the C₁ mechanism predicts a slightly lower flame speed. GRI-3.0 gives an intermediate flame speed. But on the lean H₂/air flame side, there is almost no difference in the laminar flame speed. As seen in Figs. 2 and 3, the Williams or C₂ mechanisms give the best agreement with experimental data when the stretch rate κ is below 140 s⁻¹ for $\phi=0.68$.

The flame structure near extinction ($\kappa=210$ s⁻¹) is given by Fig. 4. Although modeling results using the four mechanisms (numerical results in Fig. 4 use the Williams mechanism) show the flame temperature only drops slightly due to the high stretch rate, the experimental data show a completely different flame structure; the strong self-propagating flame is not formed at that high stretch rate. It is clear that none of the four mechanisms are appropriate for this lean, near-extinction flame. There is a big discrepancy because the numerical results indicate a

premixed flame, but actually the flame is near extinction. Therefore the flame speed, and peak temperature from experimental data are far lower than the predicted values. The actual observed flame is a so called “negative flame speed flame” [2, 3, 19] because of its formation by CH₄ fuel diffusing across the stagnation plane and reacting with the hot products from the lean H₂/air premixed flame at the other jet.

For a lean CH₄/air mixture at room temperature, the thermal diffusivity coefficient is 0.213 cm²/s and mass diffusivity (methane in air) is 0.220 cm²/s. Thus the Lewis number (the ratio of thermal diffusivity to mass diffusivity) is 0.97 and is very close to unity. Therefore the lean CH₄/air mixture has an approximately neutral preferential diffusivity, and the stretch rate will not affect the flame structure or flame speed too much [3, 9, 10]. This is true for $\kappa=90\text{ s}^{-1}$ and $\kappa=140\text{ s}^{-1}$ flames (not shown), even though peak temperature still decreases about 40 K when stretch rate changes from 90 to 140 s⁻¹. In these cases, the premixed flame is not located near the stagnation plane and can adjust its location to match the changed inlet jet velocity.

Figure 4 also shows the thermal-diffusion effect (Soret effect) on flame temperature profile ($\kappa=210\text{ s}^{-1}$, using the Williams mechanism). The numerical simulation is done by turning on and off the Soret effect. On the lean CH₄/air flame side, temperature profiles are the same with and without the Soret, but they are slightly different on the lean H₂/air flame side at the higher stretch rate. The temperature gradient on the lean H₂/air flame side contributes to the mass diffusion velocities due to the small molecular weight of the H₂ fuel.

4.2. Group B: stretched CH₄/air mixture with $\phi=0.54$ vs. hot products

The equivalence ratio for the CH₄-air flames shown in Figs. 5-7 is $\phi=0.54$ that is near the flammability limit, $\phi=0.50$. Again, the aerodynamic stretch rate varies from 90 s⁻¹ to near

extinction 210 s^{-1} . Contrary to the $\phi=0.68$ flames, lean CH_4/air premixed self-propagating flames don't exist on the CH_4/air side of the stagnation plane for each stretch rate condition for the $\phi=0.54$ CH_4/air mixture. Instead very weak “negative flame speed” flames are formed by CH_4 diffusing across the stagnation plane and reacting with the excess O_2 from the H_2/air premixed flame from the other jet [2, 3, 19]. This weak flame is located at the peak of the CO_2 profile.

The detailed flame structure for stretch rate $\kappa=140 \text{ s}^{-1}$ condition is shown in Fig. 5. Experimental measurements and numerical predictions of temperature and reactant concentrations are compared. Compared to the flame at $\kappa=90 \text{ s}^{-1}$ (not shown), the CH_4/air flame is closer to the H_2/air flame at $\kappa=140 \text{ s}^{-1}$. There is excellent agreement in the model-data comparison when using the C_2 mechanism. The peak temperature, peak CO_2 , and peak H_2O are located on the H_2/air flame side. The O_2 profile is interesting, as there is a local “bump” close to the H_2/air flame, but on the CH_4/air mixture side, the O_2 profile is very smooth. This is due to non-equidiffusion for the H_2/air mixture causing local “strengthening” of the flame. The comparison for different mechanisms is given in Fig. 6 for the same flame. For clarity, the experimental data is not shown. The predictions for T , O_2 , CO_2 , CH_4 , and H_2O based on GRI-3.0, C_1 and C_2 are almost the same (CO_2 is magnified by 10 times for good identification). The predictions based on the Williams mechanism are obviously different with that from the GRI-3.0, C_1 and C_2 mechanisms. The predicted temperature is about 40 K lower and CO_2 peak mole fraction is lower by a mole fraction value of 0.6%. In Fig. 3, predictions with the Williams mechanism show a stronger flame structure than other mechanisms. But for this very lean diffusion dominated flame, predictions with the Williams mechanism give the opposite trend.

The flame structure for $\kappa=210 \text{ s}^{-1}$ shows good agreement with the C_2 mechanism (simulation using GRI-3.0 mechanism gives similar results, not shown). The flame itself is very

similar to that for $\kappa=140 \text{ s}^{-1}$, except the reaction zone is narrower. For the diffusion flame, the flame thickness inversely scales with $\kappa^{1/2}$ [11]. Here the flame is not a pure diffusion flame, but is a “negative flame speed” CH_4/air diffusion flame formed by diffusion of a lean CH_4/air mixture into the hot products from the lean premixed H_2/air flame. But the trend is still true for this case, that is, the flame reaction zone is becoming narrower with increasing stretch rate. Incomplete reaction caused by higher stretch rate leads to lower temperature and eventual mutual flame extinction even though hot products from the lean H_2/air flame interacting downstream can extend this extinction up to a much higher level.

4.3. Group C: stretched sub-limit CH_4/air mixture vs. hot products

The lean limit for CH_4/air mixture is 5% (volume) or $\phi=0.50$. Based on the definition of flammability limit, the mixtures of $\phi=0.33$ and 0.43 studied in Figs. 8 and 9 are too lean under this limit to burn at any condition. However Ju et al. [18, 20] numerically studied the sub-limit combustion at varied stretch rate and found that some sub-limits exist. Here our planar flame experiment shows that extinction limit is dependent on external conditions such as preferential diffusion, stretch rate and support of hot products. For the CH_4/air flame, the mixture limits can go to as low of an equivalence ratio as $\phi=0.16$ if downstream hot products support the flame, even though the visible flame is very weak. Hot products commonly exist in turbulent combustion such as in combustors stabilized by recirculation zones. So this indicates the potential of sub-limit lean combustion supported by hot products.

Figure 8 shows the sub-limit flame structure of a CH_4/air mixture ($\phi=0.33$) vs. H_2/air ($\phi=0.28$) mixture ($\kappa=140 \text{ s}^{-1}$). This is a very weak negative flame speed flame. The flame temperature drops to 1300 K, just above the ignition temperature. Predictions based on GRI-3.0 (simulation using C_2 indicates no reaction) give good agreement with experiment data for

reactants and temperature. The measured CO₂ is 40% higher than predicted. Due to the low CO₂ concentration, there is some noise and uncertainty, and it is not clear if the discrepancy comes from the modeling itself or experimental uncertainty. The CO₂ mole fraction of ~ 0.6% (6000 ppm) is close the Raman detection limit.

Another sub-limit flame structure of CH₄/air ($\phi=0.43$) vs. H₂/air ($\phi=0.28$) is shown in Fig. 9. To compare the effect of the specific chemical mechanism on this sub-limit flame structure, predicted flame structures based on four different mechanisms are given (experimental data for CO₂ and temperature are shown). Again C₁, C₂ and GRI-3.0 give very similar predictions for this diffusion controlled “negative flame speed” flame. Consistent with other weak flames (Fig. 6), the Williams mechanism predicted a slightly weaker flame structure as indicated by a lower predicted peak temperature and lower predicted peak CO₂ mole fraction.

4.4. Stretch effect on CO₂ concentration and temperature

Figure 10 shows stretch effect on peak CO₂ concentration and peak temperature for flames with equivalence ratios of $\phi=0.68$ and 0.54. For equivalence ratio 0.68 flames in Fig. 10, the numerical simulation implies that there is no obvious delimit for positive self-propagating flame to negative flame speed diffusion flame. When stretch rate increases, the temperature and CO₂ peak mole fraction drops smoothly. But the experimental data show that the flame is very weak at a stretch rate of 210 s⁻¹ and the flame becomes a “negative flame speed” flame. The modeling doesn't predict the sudden drop in temperature and CO₂ that indicates a “negative flame speed” flame. For equivalence ratio $\phi=0.54$ flames, the numerical simulation implies that it is a self-propagating premixed flame at very low stretch rate (<50 s⁻¹). Although no experimental data could be obtained at this low strain rate, it is conceivable that a positive flame speed flame

can exist at the low stretch rate. When increasing stretch rate, both experimental data and predictions indicate the existence of a “negative flame speed” flame instead of the self-propagating premixed flame. There is a large drop in the CO_2 concentration at $\kappa=100 \text{ s}^{-1}$. The interesting thing is that the CO_2 concentration turns out to be constant ($\sim 1\%$) when the stretch rate is increased which means the flame strength is unchanged. The trend for temperature change with stretch is also shown in Fig. 10.

Comparison of the temperature profiles for various equivalence ratios of CH_4/air vs. lean H_2/air ($\phi=0.28$) is shown in Fig. 11. The GRI-3.0 mechanism gives a good prediction over the whole range. This clearly shows changes of the flame temperature and flame structure when changing equivalence ratio. That is, equivalence ratios 0.54 or below shows the “negative flame speed” diffusion flame formed by interaction with the hot products. When mixture equivalence ratio goes above 0.68, self-propagating flames are formed and the hot products from the H_2/air flame have little influence.

5. Summary

The flame structures of lean premixed planar CH_4/air flames, opposed by hot products produced by a lean H_2/air flame, are investigated by experiment and numerical simulation. A diffusion controlled “negative flame speed” flame exists when the premixed CH_4 mixture is very lean and it has to burn with the support from external hot products. With the support of these hot products, the lean flammability limit can be extended to a very lean range, allowing sub-limit combustion. Ultra lean CH_4/air flames ($\phi=0.33, 0.43$), which are below the flammability limit ($\phi=0.5$), are studied. Predictions with the GRI-3.0 mechanism show good agreement for most species concentration and temperature measurement even though there is some discrepancy in

the CO₂ profile for the two sub-limit flames. The CO₂ peak mole fraction is approximately 1% for these ultra-lean flames. Predictions of CO₂ profiles based on the Williams mechanism are substantially lower than those by the GRI-mechanism.

Lean CH₄/air ($\phi=0.54$) flames, above the flammability limit ($\phi=0.5$), supported by hot products show the downstream interaction supports a very weak diffusion flame by supplying high temperature products or flame radicals. From low stretch rate to near extinction, numerical simulations with C₂, C₁ and GRI-3.0 show good agreement with experimental data. Simulation with the Williams mechanism predicts a slightly low CO₂ peak compared to other mechanisms. But there is an opposite trend for self-propagating flames with equivalence ratio of 0.68. Lean CH₄/air ($\phi=0.68$) flames supported by downstream hot products show very good agreement between experimental data and numerical results when the stretch rate is below 140 s⁻¹. The Williams mechanism and C₂ mechanism give better predictions than C₁ or GRI-3.0. The Williams mechanism predicts a higher flame speed and gives the best agreement with the experiment data for self-propagating, low stretch rate flames at $\phi=0.68$ CH₄/air mixtures. But when the stretch rate is increased to 210 s⁻¹, the observed flame structure is completely different from that predicted by all four mechanisms. The simulations predict a self-propagating flame and the experiment shows a “negative flame speed” flame.

Acknowledgements

This work is partly supported by the U.S. Department of Energy's Office of Basic Energy Sciences, Partnerships for Academic-Industrial Research (PAIR) grant (No. DE-FG02-98ER14915), with Dr. Alan H. Laufer as the technical monitor.

REFERENCES

1. D.C. Haworth, R.J. Blint, B. Cuenot, and T.J. Poinso, *Combust. Flame* 121 (3) (2000) 395-417.
2. S.H. Sohrab, Z.Y. Ye, C.K. Law, *Proc. Combust. Inst.* 20 (1984) 1957-1965.
3. C.K. Law, *Proc. Combust. Inst.*, 22 (1988) 1381-1402.
4. D.M. Mosbacher, J.A. Wehrmeyer, R.W. Pitz, C.J. Sung and J.L. Byrd, *Proc. Combust. Inst.* 29 (2002) 1479-1486.
5. M.A. Tanoff, M.D. Smooke, R.J. Osborne, T.M. Brown, R.W. Pitz, *Proc. Combust. Inst.* 26 (1996) 1121-1128.
6. R.S. Barlow, A.N. Karpetis, J.H. Frank, and J.-Y. Chen, *Combust. Flame* 127 (2001) 2102-2118.
7. J.A. Wehrmeyer, Z. Cheng, D.M. Mosbacher, R.W. Pitz, and R. Osborne, *Combust. Flame* 128 (3) (2002) 232-241.
8. Z. Cheng, J.A. Wehrmeyer, and R.W. Pitz, 38th AIAA/ASME/SAE/ASEE Joint Propulsion Conference, AIAA 2002-4021, Indianapolis, IN, 2002.
9. C.J. Sung, J.B. Liu, and C.K. Law, *Combust. Flame* 106 (1-2) (1996) 168-183.
10. C.K. Law, C.J. Sung, G. Yu and R.L. Axelbaum, *Combust. Flame* 98 (1-2) (1994) 139-154.
11. C.J. Sung, G. J.B. Liu, and C.K. Law, *Combust. Flame* 102 (4) (1995) 481-492.
12. K. Seshadri, I. Puri, and N. Peters, *Combust. Flame* 61 (3) (1985) 237-249.
13. R.J. Kee, F.M. Rupey, J.A. Miller, M.E. Coltrin, J.F. Grcar, E. Meeks, H.K. Moffat, A.E. Lutz, G. Dixon-Lewis, M.D. Smooke, J. Warnatz, G.H. Evans, R.S. Larson, R.E. Mitchell, L.R. Petzold, W.C. Reynolds, M. Caracotsios, W.E. Stewart, and P. Glarorg, C. Wang,, O. Adigum, W.G. Houf, C.P. Chou, and S.F. Miller, Chemkin Collection, Release 3.7, Reaction Design, Inc., San Diego, CA (2002).
14. Peters, N., *Reduced Kinetic Mechanisms for Applications in Combustion Systems* in: N. Peters and B. Rogg (Eds.), *Lecture Notes in Physics*, Springer-Verlag, Berlin, Vol. M15, 1992, Ch. 1, p. 3-12.
15. G.P. Smith, D.M. Golden, M. Frenklach, N.W. Moriarty, B. Eiteneer, M. Goldenberg, C.T. Bowman, R.K. Hanson, S. Song, W.C. Jr. Gardiner, V.V. Lissianski, and Z. Qin, <http://www.me.berkeley.edu/gri-mech>.

16. <http://maeweb.ucsd.edu/~combustion/cermech>.
17. I. Glassman, *Combustion*, Third edition, Academic Press, San Diego, CA, 1996.
18. Y. Ju, H. Guo, K. Maruta, and T. Niioka, *Combust. Flame* 113 (4) (1998) 603-614.
19. N. Darabiha, C.M Candel, and F.E. Marble, *Combust. Flame* 64 (2) (1986) 203-217.
20. Y. Ju, H. Matsumi, K. Takita, and G. Masuya, *Combust. Flame* 116 (4) (1999) 580-592.

List of Figures

1. Representative Raman spectra obtained from the flame shown in Fig. 2. Spectra correspond to two axial positions along the centerline of the opposed jet burner where “x” is the distance from the top jet.
2. Experimental and numerically-predicted species and temperature profiles for: CH₄/air ($\phi=0.68$) vs. H₂/air ($\phi=0.28$), $\kappa=140\text{ s}^{-1}$.
3. Numerically-predicted species and temperature profiles using four different mechanisms for: CH₄/air ($\phi=0.68$) vs. H₂/air ($\phi=0.28$), $\kappa=140\text{ s}^{-1}$.
4. Experimental and numerically-predicted species and temperature profiles for: CH₄/air ($\phi=0.68$) vs. H₂/air ($\phi=0.28$), $\kappa=210\text{ s}^{-1}$. Numerical simulation uses the Williams mechanism.
5. Experimental and numerically-predicted species and temperature profiles: CH₄/air ($\phi=0.54$) vs. H₂/air ($\phi=0.28$), $\kappa=140\text{ s}^{-1}$.
6. Numerically-predicted species and temperature profiles using four different mechanisms for: CH₄/air ($\phi=0.54$) vs. H₂/air ($\phi=0.28$), $\kappa=140\text{ s}^{-1}$.
7. Experimental and numerically-predicted species and temperature profiles for: CH₄/air ($\phi=0.54$) vs. H₂/air ($\phi=0.28$), $\kappa=210\text{ s}^{-1}$.
8. Experimental and numerically-predicted species and temperature profiles for: CH₄/air ($\phi=0.33$) vs. H₂/air ($\phi=0.28$), $\kappa=140\text{ s}^{-1}$.
9. Numerically-predicted species and temperature profiles using four mechanisms for: CH₄/air ($\phi=0.43$) vs. H₂/air ($\phi=0.28$), $\kappa=140\text{ s}^{-1}$. Experimental data for CO₂ and temperature are shown.
10. Experimental and numerically-predicted CO₂ peak concentration and peak temperature at various stretch rate for: CH₄/air ($\phi=0.54$ or 0.68) vs. H₂/air ($\phi=0.28$), $\kappa=140\text{ s}^{-1}$. Numerical simulation uses GRI-3.0.
11. Experimental and numerically-predicted temperature profiles for different equivalence ratio of CH₄/air vs. H₂/air ($\phi=0.28$), $\kappa=140\text{ s}^{-1}$. Numerical simulation uses GRI-3.0.

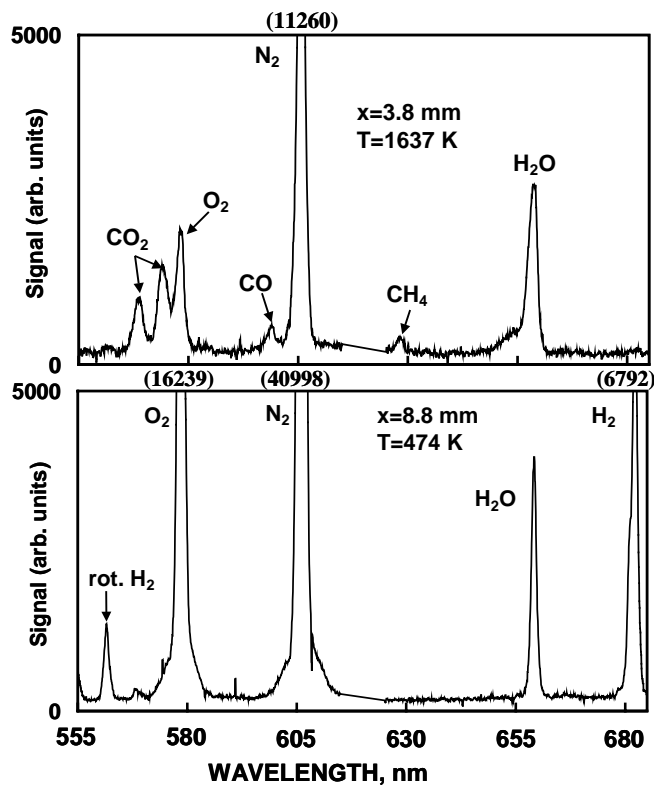


Fig. 1. Representative Raman spectra obtained from the flame shown in Fig. 2. Spectra correspond to two axial positions along the centerline of the opposed jet burner where “x” is the distance from the top jet.

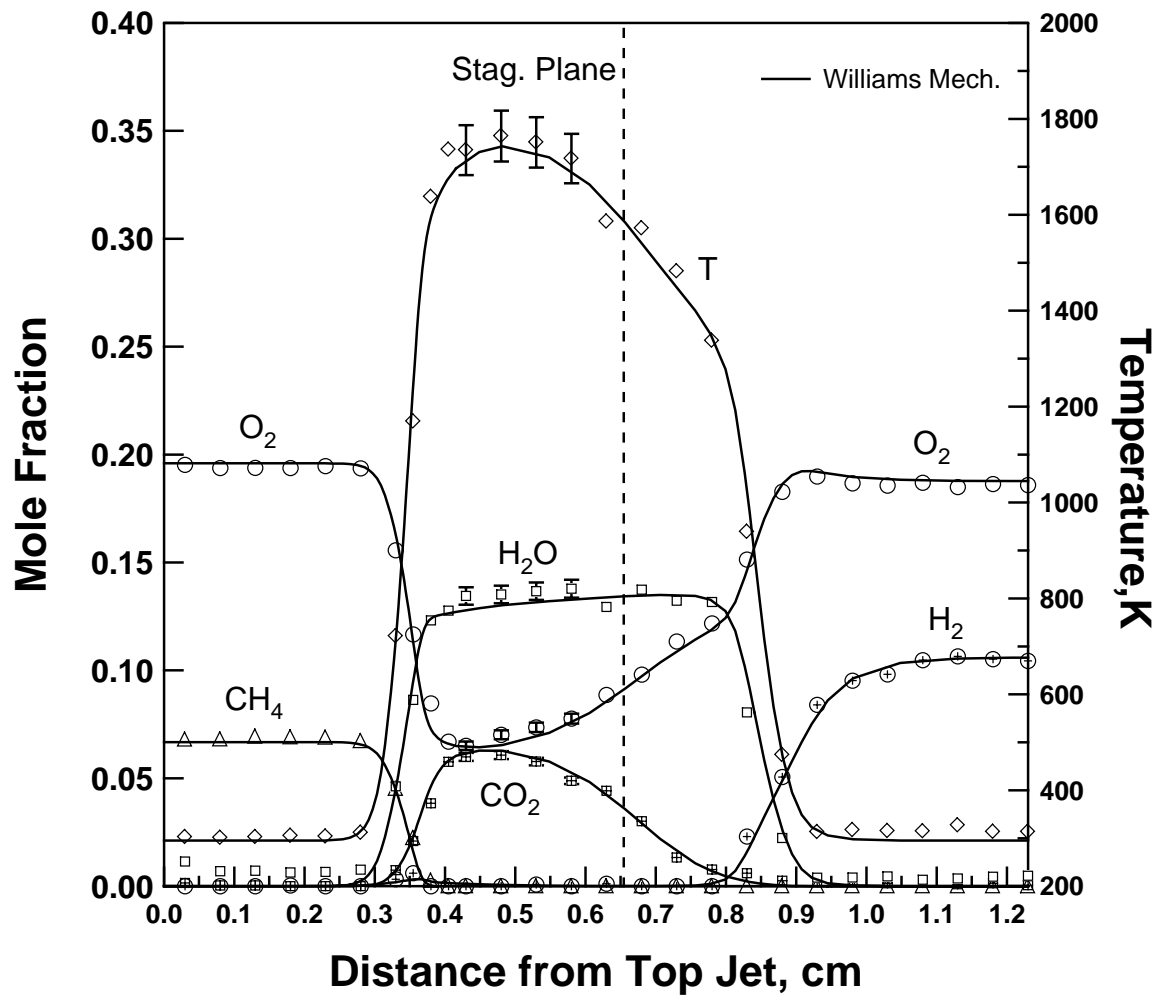


Fig. 2. Experimental and numerically-predicted species and temperature profiles for: CH₄/air ($\phi=0.68$) vs. H₂/air ($\phi=0.28$), $\kappa=140 \text{ s}^{-1}$.

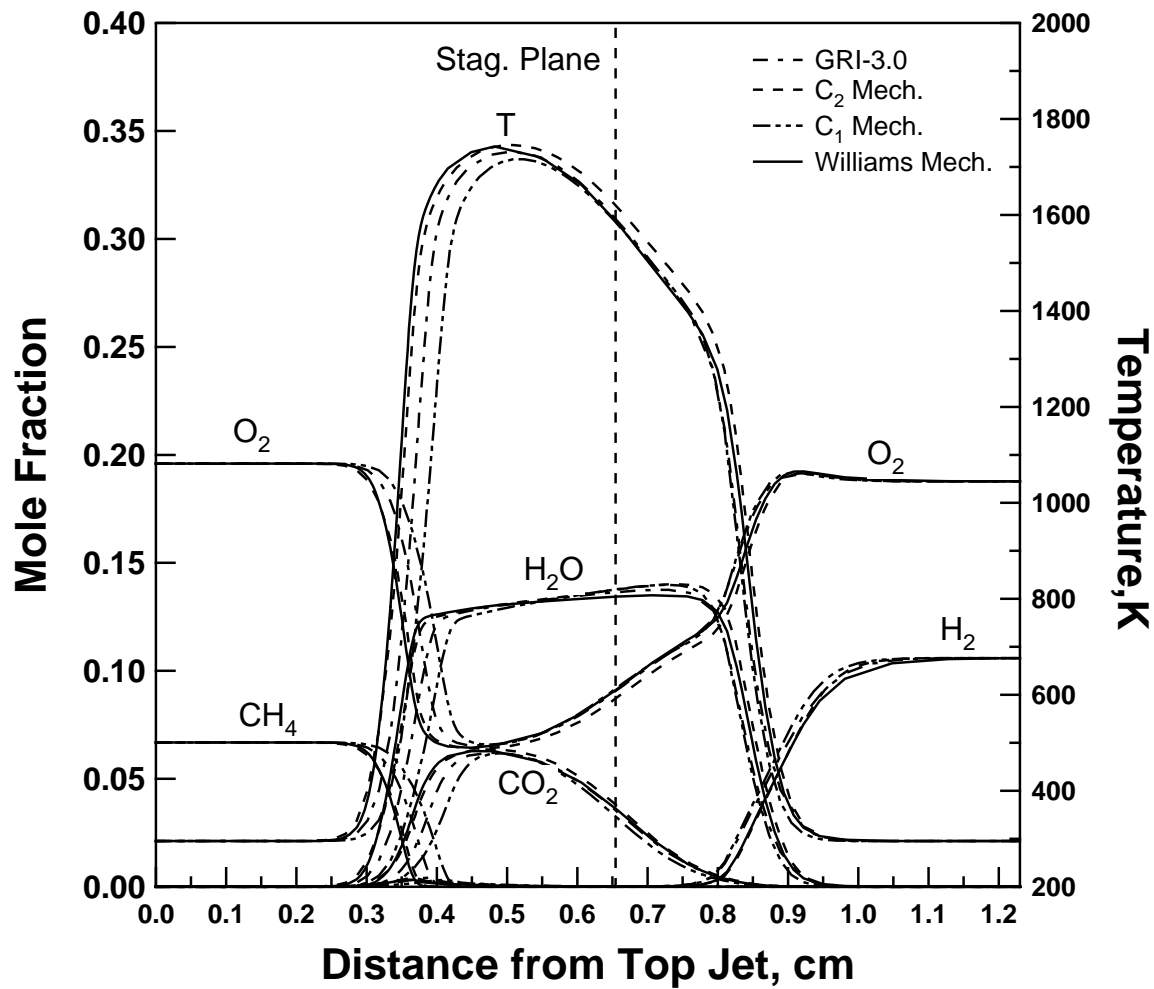


Fig. 3. Numerically-predicted species and temperature profiles using four different mechanisms for: CH₄/air ($\phi=0.68$) vs. H₂/air ($\phi=0.28$), $\kappa=140 \text{ s}^{-1}$.

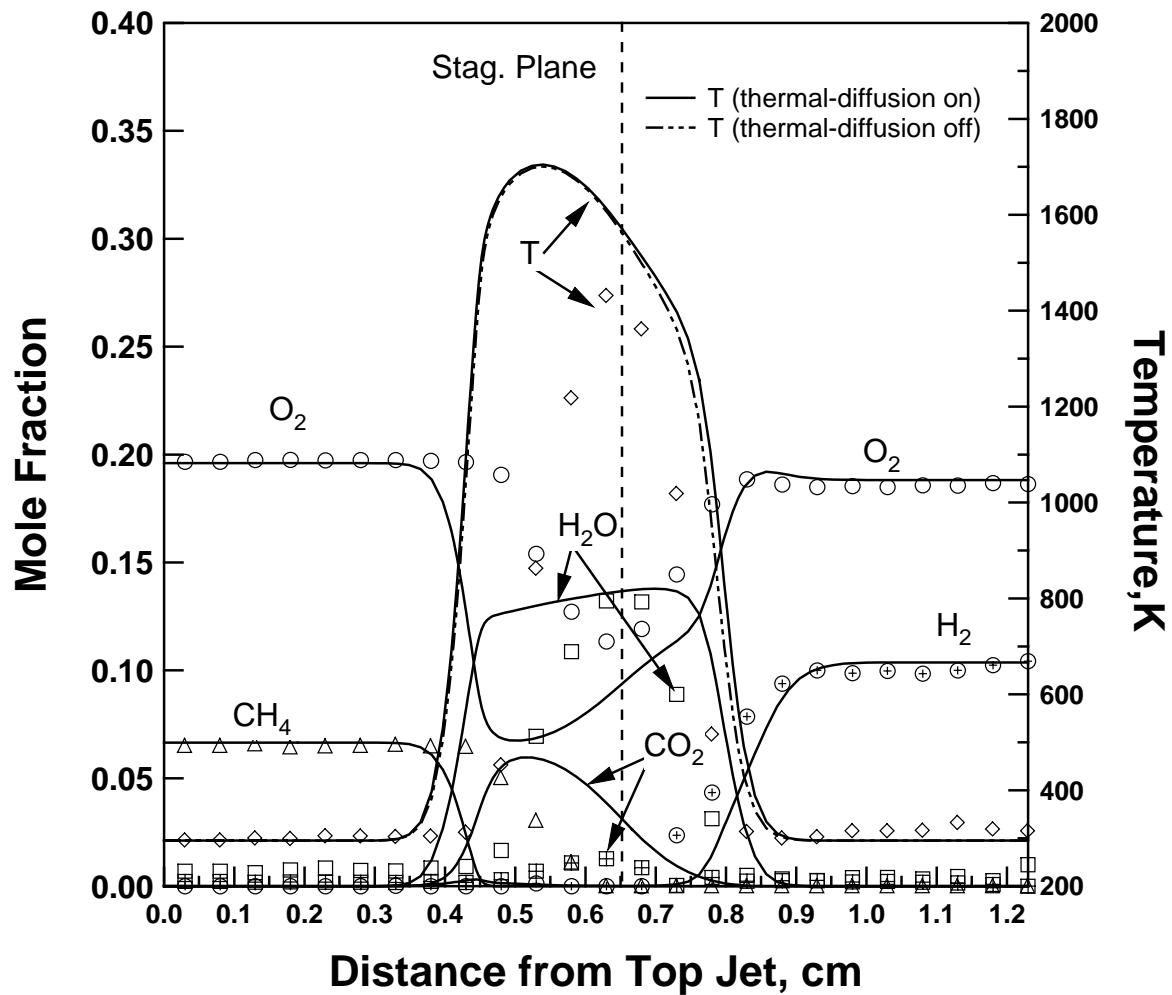


Fig. 4. Experimental and numerically-predicted species and temperature profiles for: CH₄/air ($\phi=0.68$) vs. H₂/air ($\phi=0.28$), $\kappa=210 \text{ s}^{-1}$. Numerical simulation uses the Williams mechanism.

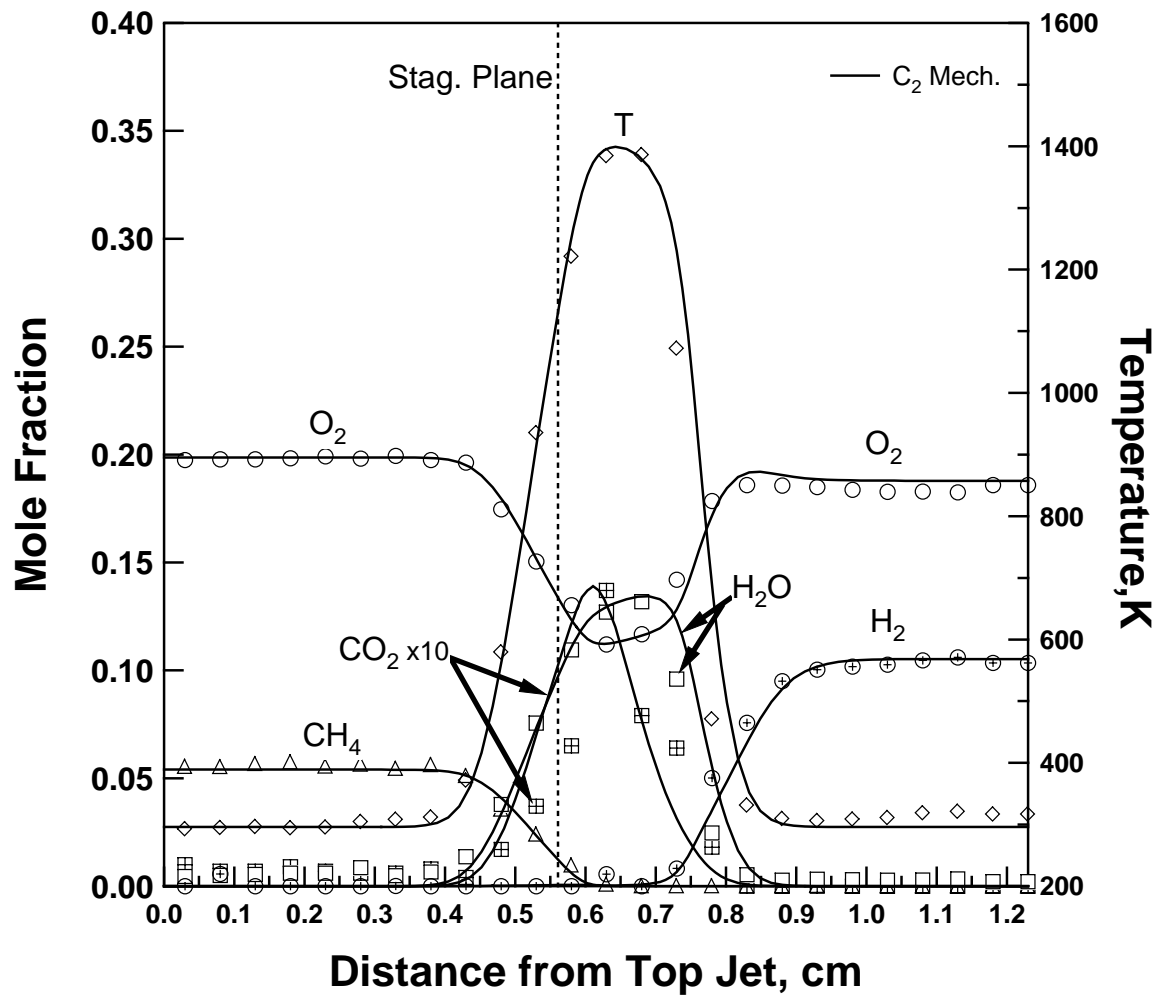


Fig. 5. Experimental and numerically-predicted species and temperature profiles for: CH₄/air ($\phi=0.54$) vs. H₂/air ($\phi=0.28$), $\kappa=140 \text{ s}^{-1}$.

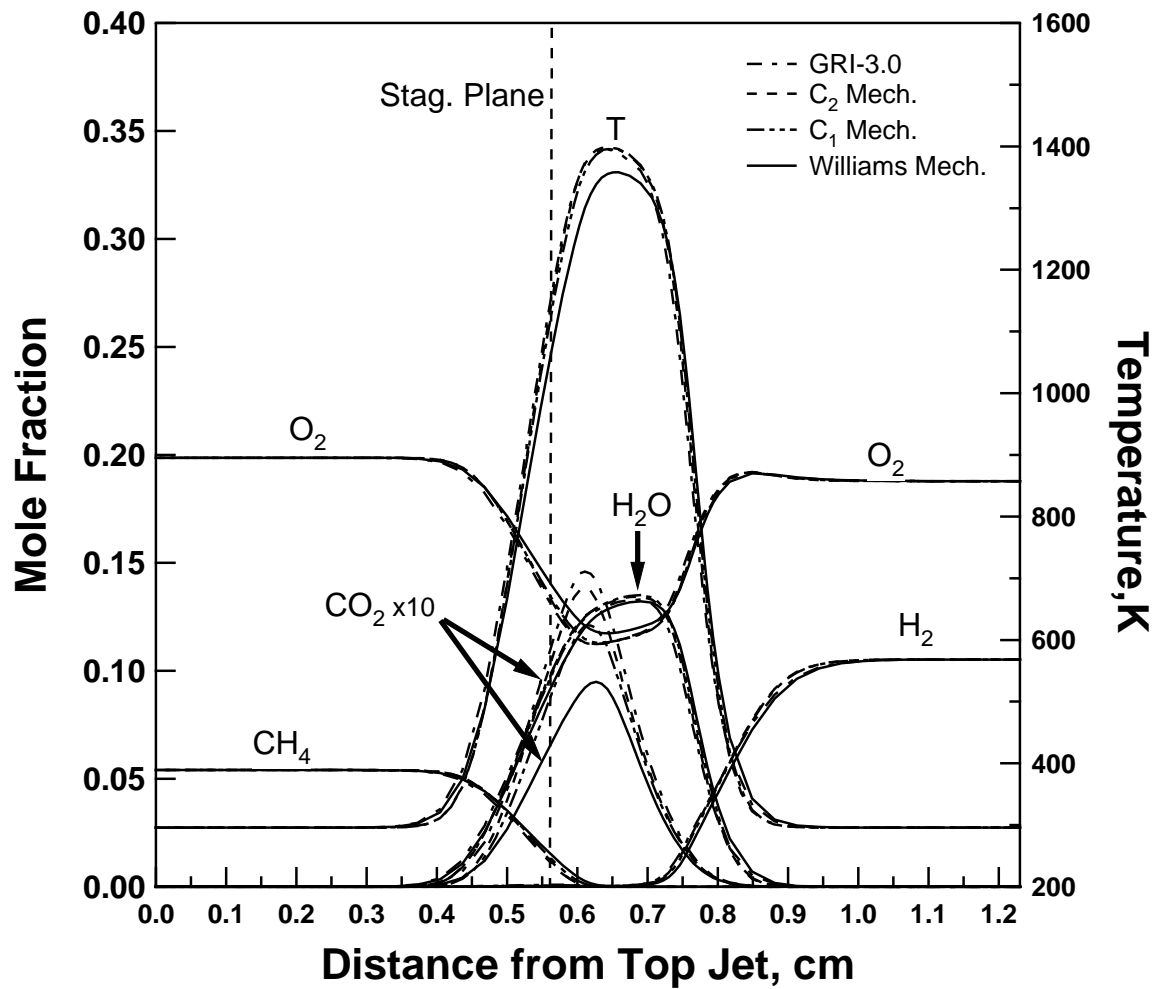


Fig. 6. The comparison of numerically-predicted species and temperature profiles using four different mechanisms for: CH₄/air ($\phi=0.54$) vs. H₂/air ($\phi=0.28$), $\kappa=140 \text{ s}^{-1}$.

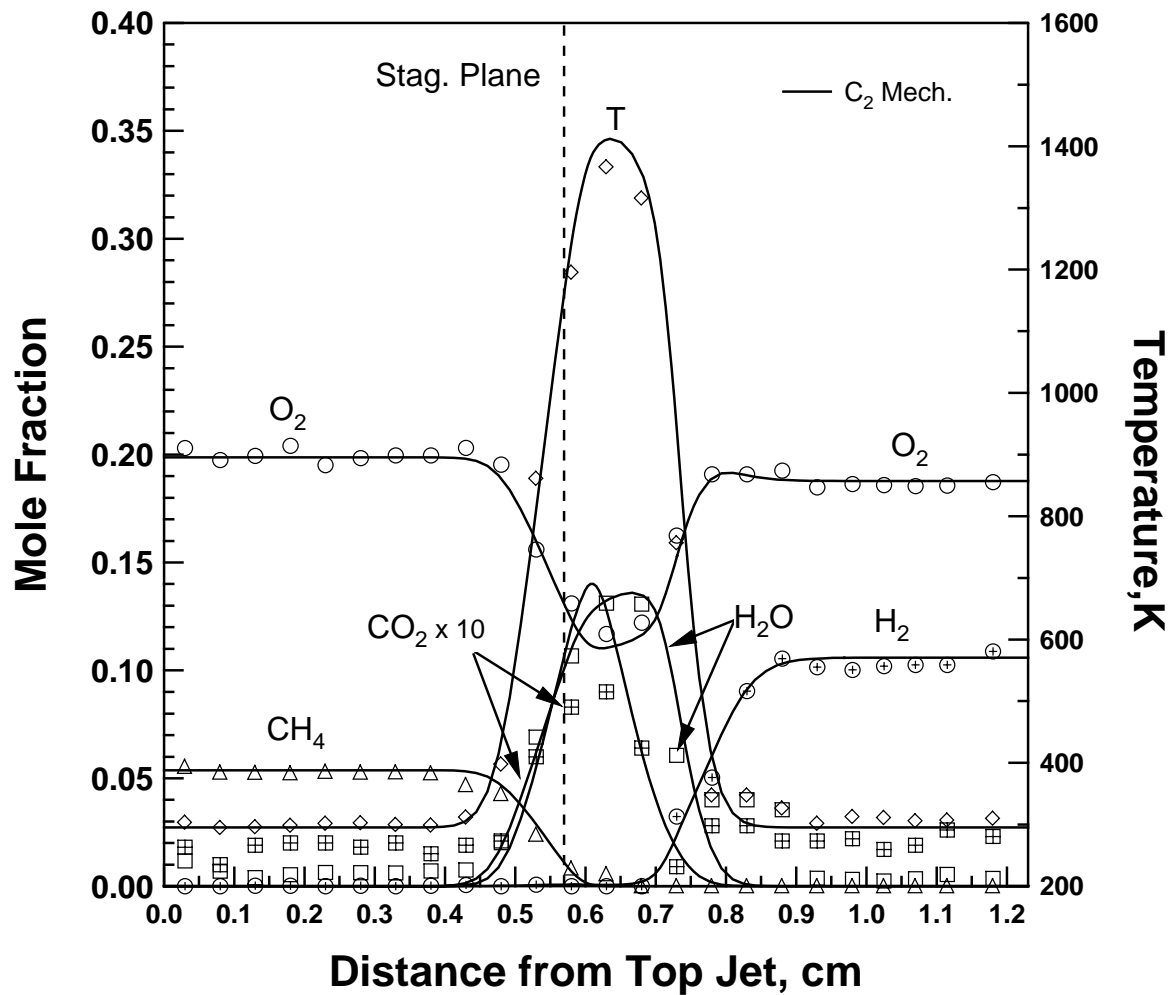


Fig. 7. Experimental and numerically-predicted species and temperature profiles for: CH_4/air ($\phi=0.54$) vs. H_2/air ($\phi=0.28$), $\kappa=210 \text{ s}^{-1}$.

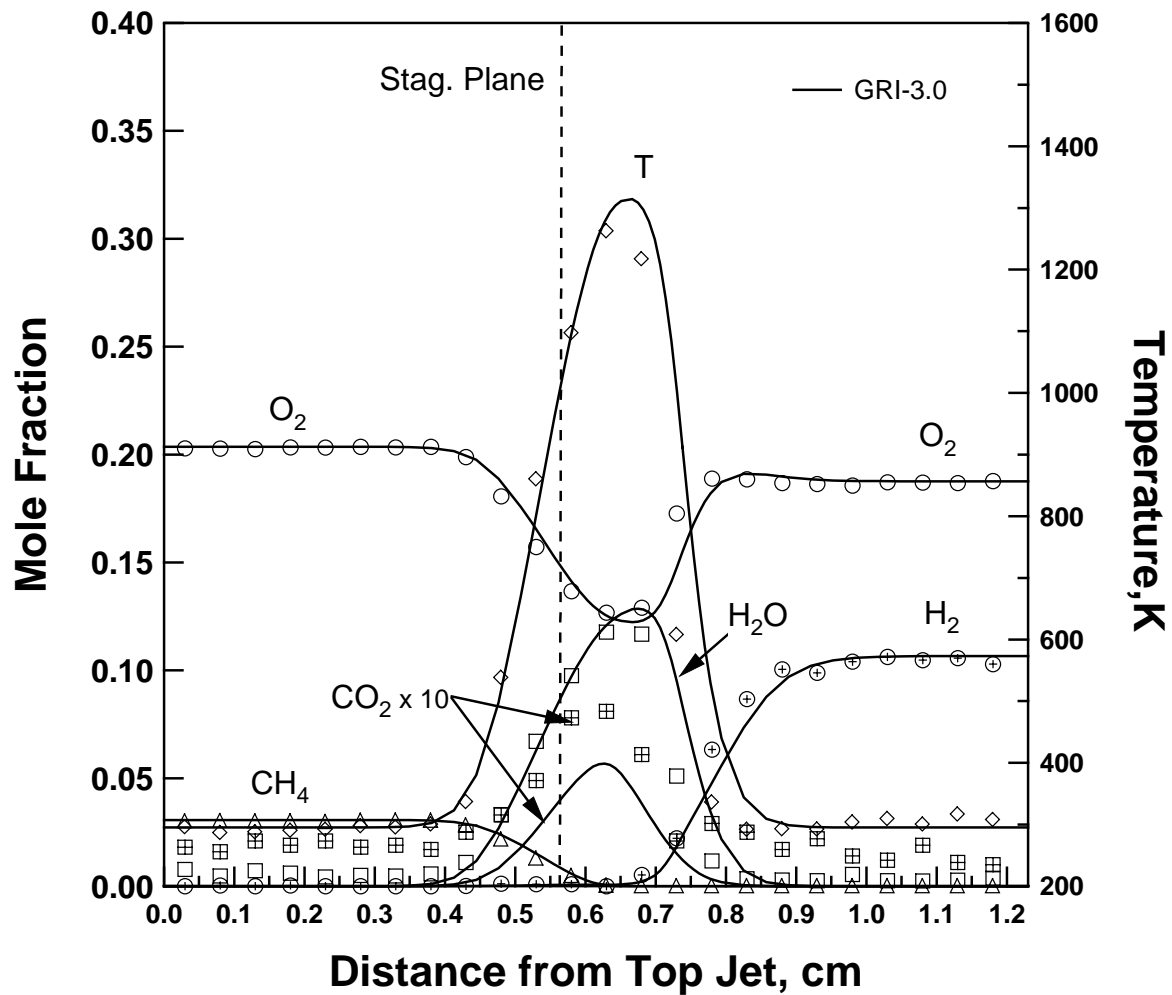


Fig. 8. Experimental and numerically-predicted species and temperature profiles for: CH₄/air ($\phi=0.33$) vs. H₂/air ($\phi=0.28$), $\kappa=140 \text{ s}^{-1}$.

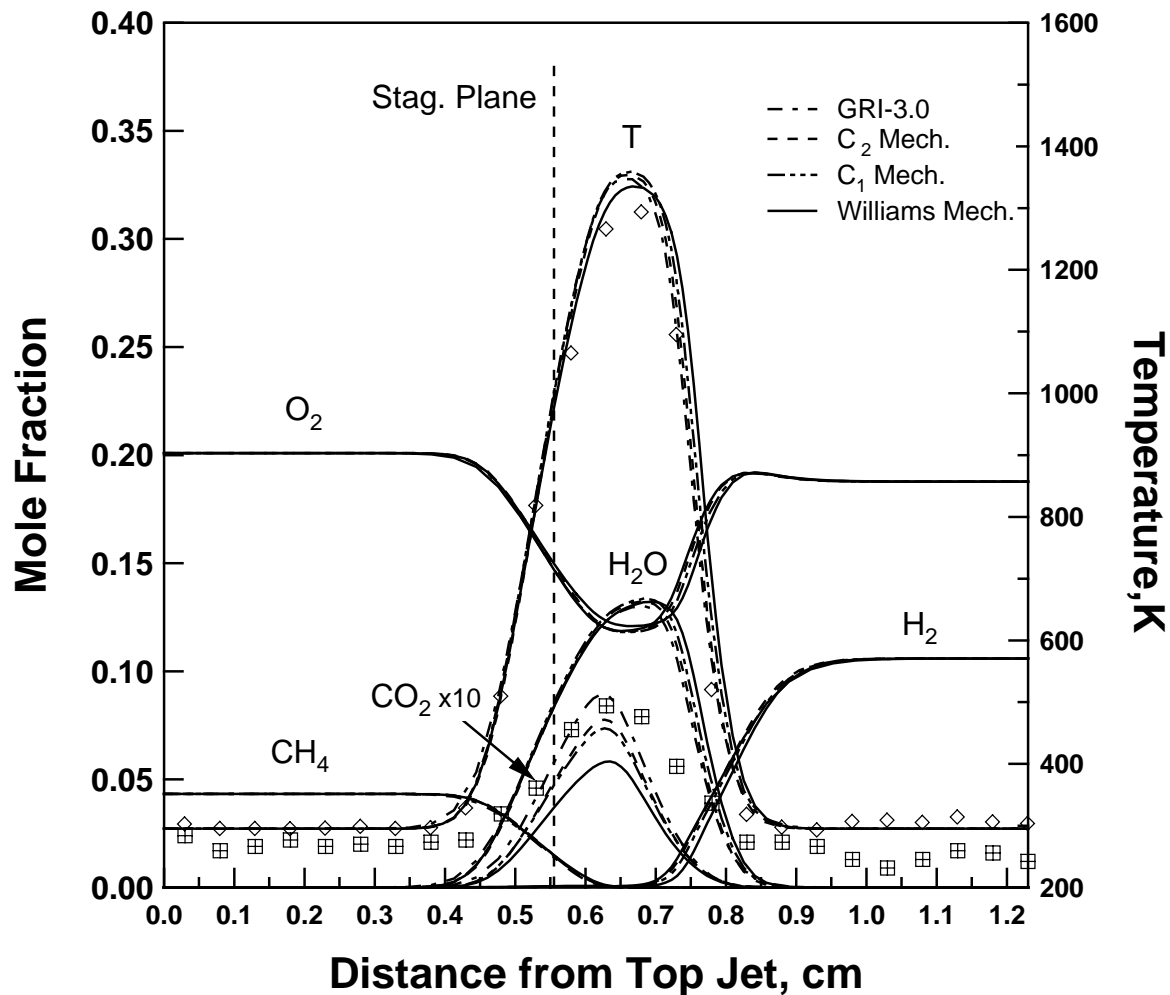


Fig. 9. The comparison of numerically-predicted species and temperature profiles using four mechanisms for: CH₄/air ($\phi=0.43$) vs. H₂/air ($\phi=0.28$), $\kappa=140 \text{ s}^{-1}$. Experimental data for CO₂ and temperature are shown.

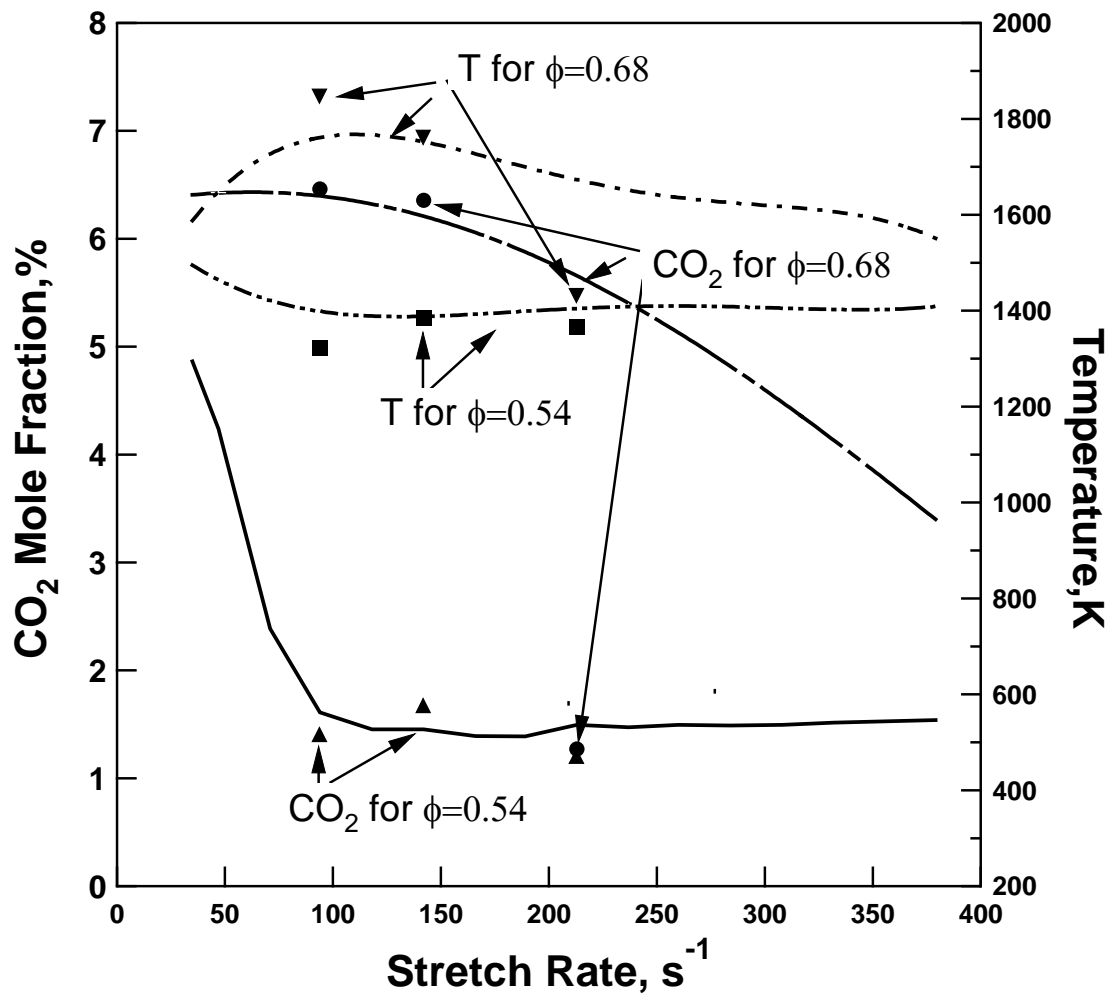


Fig. 10. Experimental and numerically-predicted CO_2 peak concentration and peak temperature at various stretch rate for: CH_4/air ($\phi=0.54$ or 0.68) vs. H_2/air ($\phi=0.28$), $\kappa=140 s^{-1}$. Numerical simulation uses GRI-3.0.

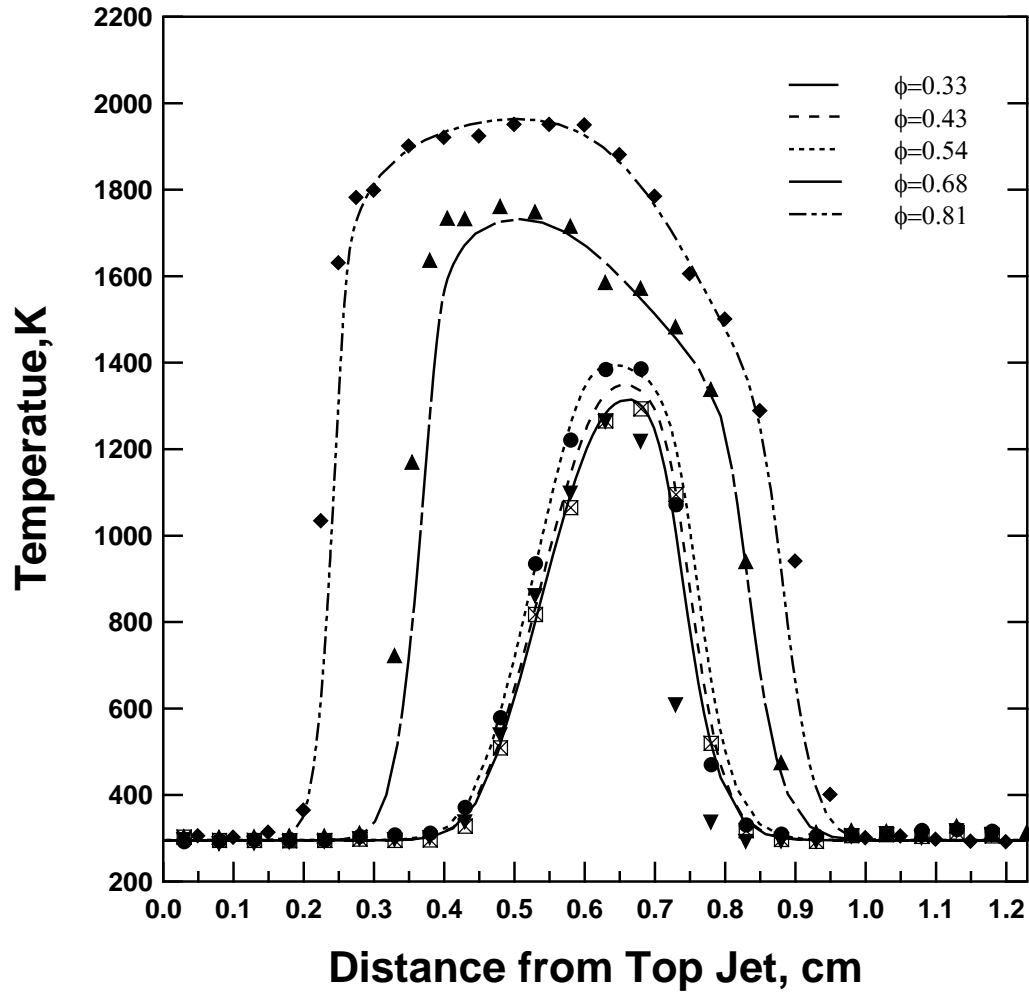


Fig. 11. Experimental and numerically-predicted temperature profiles for different equivalence ratio of CH_4/air vs. H_2/air ($\phi=0.28$), $\kappa=140 \text{ s}^{-1}$. Numerical simulation uses GRI-3.0.